A Mathematical Model of the External Circuits in a Bipolar Membrane Electrodialysis Stack: Leakage Currents and Joule Heating Effect

Zheng Peng [a], Yue Sun [a,*], Peixin Shi [a], Yuanyuan Wang [a]

[a] Department of Municipal Engineering, School of Civil Engineering, Southeast University, Nanjing 211189, China

*Corresponding author. E-mail: yuesun@seu.edu.cn.

Abstract: Leakage currents existing in a bipolar membrane electrodialysis (EDBM） stack cause loss of coulombic efficiency, ranged from approximately 0.9% to 12%, and create undesirable heat that impairs its operation. A model for predicting leakage currents in a EDBM stack was developed by considering the electrochemical process as an electrical analog circuit. Current and potential balance equations are used to define the equivalent network, and differential calculus is used to solve these equations. Leakage currents model is validated with experimental and simulated results. On this basis, leakage currents and Joule heating effect in a pilot-scale EDBM stack are analyzed. The results reveal that leakage currents in external circuits are distributed symmetrically around the membrane stack and are significantly affected by the number of cell pairs, current density, and element resistivity. Moreover, Joule heating effect in the external circuit in the stack is quantitatively analyzed and the temperature effect is dominated by the slot closed to the electrode cell in the acid compartment. This was most pronounced (raised by 12.18 ℃ in 0.3 s) during the termination stage. Using these findings, EDBM stacks can be improved and the optimal spacers and a more reasonable process can be designed, which could boost the development of EDBMs.

Key words: Bipolar Membrane Electrodialysis, Producing Acid and Base, Leakage Currents, Differential Calculus, Joule heating effect

1. Introduction

Industrial ecology and sustainability have been a topic of growing interest in recent years [1]. Recently, bipolar membranes (BPMs) integrated with sustainable advanced processes such as artificial photosynthesis, hydrogen evolution reactions, oxygen evolution reactions, and CO_2 photoreduction, are attracting more attention due to achieving long-term optimal pH conditions[2], owing to their ability to generate H^+/OH^- ions *in situ* without the need to introduce additional salt [3]. Its theoretical potential is 0.83 V at 298 K [4, 5], which is much lower than the potential of water electrolysis for producing an acid and base (2.06 V) [6, 7]. Due to these unique advantages, BPMs can also be integrated into conventional electrodialysis (CED) processes, so called electrodialysis with bipolar membranes (EDBM), to attain a salt conversion or provide H^+ and OH^- ions [2]. EDBM therefore also has immense potential for numerous industrial processes including the conversion of concentrated salt solutions into acids and bases [8, 9], acidification and alkalization of milk or juice [10], continuous regeneration of ion exchange resins *in situ*

[11], and recovery of inorganic or organic matter in effluent [12]. In these processes, there is no salt by-product due to water splitting into H^+/OH^- ions, and the H^+/OH^- ions combining to form water. Even the waste materials are used as feedstock, and in resource regeneration and effluent treatment. In a sense, EDBM plays a role as a "photo-synthesizer" in industrial ecosystems to realize closed loops in the production process [13], meeting the goal of industrial ecology.

As for most electromembrane processes, EDBM stack design is based on the use of plate-and-frame geometries, in which compartments consist of two membranes with a non-metallic spacer forming the interspace between them [14]. Each spacer has several slots and ducts to distribute or converge the solutions, and these slots and ducts form so called "liquid bridges." Electrical currents flow through them due to an existing potential difference between adjacent cells. These currents, also called leakage currents, bypass the effective area of the membranes, often resulting in losses of coulombic efficiency [15]. The total effective electrical leakage in a CED stack ranges from approximately 0.9% to 12%. Details are shown in Table S1 [16-19]. These noneffective currents are not used for the migration of target ions but generate Joule heat in external circuits. It is interesting that Joule heat does not decrease progressively as the leakage currents decrease, as shown in Fig. S1. Leakage currents of independent hydraulic circuits are difficult to manage in practice, especially for an industrial-scale stack, that an exact model needs to be applied to describing it and its effects. Heretofore, several simplified models based on Wilson current leakage equations have been widely used to calculate current leakage ratios in the field of CED [16-18, 20]. In the Wilson's model in a CED system, a single loop circuit model of leakage currents is established by neglecting the potential difference between adjacent compartments [16]. The hydraulic circuits structure of a EDBM system is different from a CED system as well as the elements in the stack, as shown in Fig. 1. These models developed for a CED system are no longer applicable to describing leakage currents occurring in EDBM systems. To analyze these phenomena that occurred in a EDBM system during the EDBM process, an electrical analog circuit of a lab-scale system with three-compartment was initially investigated by using Software Multisim [21]. During the EDBM process, the variation characteristics of the leakage circuit contained the electrical resistance, voltage, current and thermal effect of the slots/ducts were presented in a lab-scale system. Although the leakage circuit characteristics was described in detail during the EDBM process, these findings were based on a small-scale stack under a constant current density. From a small-scale stack to an industrial-scale stack, the leakage currents would be magnified, and Joule heating effect phenomenon was most pronounced in the industrial-scale stack. Meanwhile, the Software Multisim can be applied to analyze a small-scale circuit (around 10 cell pairs or less), but it cannot be adopted to simulate a large-scale circuit (around 500 cell pairs or more) in an

industrial-scale stack. Thus, it is quite necessary to develop a mathematical model for describing the quantitative relationship among the factors and currents leakage/Joule heating effect phenomenon, especially for an industrial-scale stack. It is well known that the model development aims not only to predict experimental results but also a better understanding of the processes involved to optimize the technique [7], such as assessing a EDBM stack, optimizing the type of spacers, and designing the EDBM process.

A EDBM stack contains N-units with three-compartment configurations that are often chosen to meet the practical requirements for producing an acid and base, as exhibited in Fig. 1B. Stack forms three independent hydraulic circuits and presents different characteristics to the external circuits in the EDBM stack. In our study, we developed the leakage current equation for individual hydraulic circuits and the Joule heating effect model for the ducts and slots at the spacer. First, the subcomponents of the EDBM process are systematically analyzed EDBM and mathematical expressions are established based on an electrical analogy for each subcomponent factor. Second, an equivalent electrical model of three hydraulic circuits in a EDBM stack is depicted as a complex 2 × N-rank network, and thereafter, simplified to a complex 1 × N-rank network. Third, the current balance and potential balance equations are applied to the complex 1 × N-rank network and a general solution is obtained by using differential calculus. Finally, the Joule heating effect on the external circuits is quantitatively analyzed by proposing a thermoelectric conversion model. Furthermore, these models are validated using experimental and simulation results. On this basis, the leakage currents in a pilot-scale EDBM stack are analyzed in terms of their distribution, resistive elements, number of cell pairs, and current density. The Joule heating effect on the external circuit in the pilot-scale EDBM stack is predicted after producing acid and base and some measures were proposed to minimize the effect. The findings of this work will help to assess the leakage currents when designing EDBM stack so they can be minimized for when the system is built.

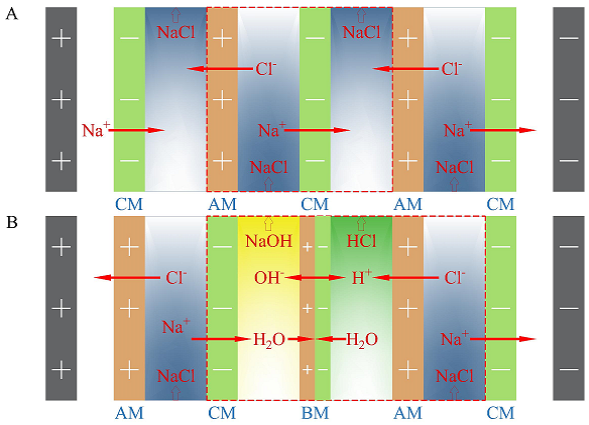

Fig. 1. Structure of ED and EDBM stack. A. ED. B. EDBM.

2. Model description

2.1. Composite cell pair resistance

A repeating unit in the EDBM stack, namely a cell pair, consists of a bipolar membrane (BPM), a base compartment, a cation exchange membrane (CM), a feed compartment, an anion exchange membrane (AM), and an acid compartment in sequence, as depicted in Fig. S2. Therefore, a composite cell pair resistance, including membrane resistances and bulk stream resistances, is related to the geometry and conductivity of the solution. Based on an extension of the Teorell-Meyer-Sievers theory [14], two concentration diffusion boundary layers (DBLs) flanking the membranes exist as shown in Fig. S3. The presence of the DBLs can significantly affect the total voltage drop of the membrane stack. The DBL thickness can be partially decreased by increasing the turbulence in the channels, and nevertheless it is not completely eliminated [22]. Hence, the bulk stream resistances, $\boldsymbol{R_C}$, in the compartments can be given as [23, 24]:

$$R_C = \frac{1}{\varepsilon^2}\left(\frac{h - 2\sigma}{\overline{\Lambda}\, A} + \frac{2\sigma}{\overline{\Lambda^{\mathrm{DBL}}}\, A}\right) \tag{1}$$

where $\overline{\Lambda}$ is the average conductivity of the bulk stream except for the diffusion boundary layer. $\overline{\Lambda^{\mathrm{DBL}}}$ is the average conductivity of the bulk stream in the diffusion boundary layer, as shown in Appendix A. h is the thickness of each compartment. σ is the thickness of the diffusion boundary layer, typically in the range 100 μm to 200 μm [22]. A is the effective area of the membrane. ε is the porosity of the spacer (the porosity is squared to reflect the tortuous ion transport), defined as [24]:

$$\varepsilon = 1 - \frac{\pi d_f^2}{2 l_f h} \tag{2}$$

where d_f is the filament diameter in the spacer. l_f is the filament pitch in the spacer.

Membrane resistance is strongly affected by the electrolyte concentration, and is the most difficult term to calculate accurately [25]. Generally, a constant value given by the membrane manufacturer is used for membrane resistance [26, 27]. However, membrane resistance varies as the solution concentration on either side of the membranes varies during the EDBM process. Efforts have been made in previous studies to provide a more accurate measure for membrane resistance for practical applications [25, 28, 29]. Electrochemical impedance spectroscopy can be used to measure the true membrane resistance [28], but its operation is more complex than that of theoretical models. Galama et al.[25] developed a membrane resistance model for the anion/cation membranes (AM/CM) that divided the membrane resistance into two terms, one depending on the external salt concentration, and one independent of the external salt concentration. Hence AM/CM resistance can be expressed as:

$$R_{\mathrm{AM/CM}} = \frac{1}{(1 - f)}\left(\frac{1}{\Lambda_I} + \frac{1}{\Lambda_{II} k_{\mathrm{ext}}}\right)\frac{1}{A} \tag{3}$$

$$(f)_{\max} = 1 - \frac{A_{\mathrm{OP}}}{A_{\mathrm{TO}}} \tag{4}$$

where f is the portion of the membrane area that is masked by the spacer, and referred to as the shadow factor. $A_{\mathrm{OP}}/A_{\mathrm{TO}}$ is the ratio of the open area to the total area in the spacers [23, 30]. Λ_I and Λ_{II} are constants that represent the conductance resulting from the ions in the micro-cavities and micro-channels [25]. k_{ext} is the dimensionless external concentration, obtained from dividing C_{ext} by the reference concentration C_0 = 1 M. When the solution concentration flanked the membranes differ, the concentration profile in the membrane is described as:

$$\overline{C}(x) = C_{\mathrm{low}} + (C_{\mathrm{high}} - C_{\mathrm{low}})\left(\frac{x}{\delta}\right)^n \tag{5}$$

where x is the position in membrane. δ is the membrane thickness. n is a fit parameter that describes the concentration profile between two points as dictated by the two external solution concentrations.

The structure of the BPM is described as one cation exchange layer (CEL), one anion exchange layer (AEL) and an interfacial layer (IL) between them. Under the directed current field, water splitting occurs at the interfacial layer, and generates protons and hydroxide ions through the CEL and the AEL, respectively. The BPM resistance can be divided into three terms, the resistance of the CEL, the resistance of the AEL, and the resistance of the IL. It is assumed that only deionized water exists in the IL, so its resistance can be expressed as [31, 32]:

$$r_{\mathrm{IL}} = \frac{\lambda}{F(C_{H^+} u_{H^+} + C_{\mathrm{OH}^-} u_{\mathrm{OH}^-})} = \frac{\lambda}{(C_{H^+} \Lambda_{H^+} + C_{\mathrm{OH}^-} \Lambda_{\mathrm{OH}^-})} \tag{6}$$

$$R_{\mathrm{BPM}} = \frac{1}{1 - f}(r_{\mathrm{CEL}} + r_{\mathrm{IL}} + r_{\mathrm{AEL}})\frac{1}{A} \tag{7}$$

where r_{CEL}, r_{AEL}, and r_{IL} represents the CEL resistance, the AEL resistance, and the IL resistance, respectively. λ s the thickness of the IL. C_{H^+}, and C_{OH^-} is the concentrations of H^+, and OH^- ions, respectively. u_{H^+}, and u_{OH^-} is the mobility of H^+, and OH^- ions, respectively. Λ_{H^+}, and Λ_{OH^-} is the conductivity of H^+, and OH^- ions, respectively.

2.2. Membrane potential

When an ion exchange membrane (IEM) is immersed between two electrolytes at different concentrations, a potential is generated over its two sides, as shown in Fig. S4. According to the Teorell-Meyer-Sievers theory, the membrane potential can be expressed as [14, 33]:

$$E_{\mathrm{IEM}} = E_{\mathrm{Don}}^{L} - E_{\mathrm{Don}}^{R} + E_{\mathrm{diff}} = \frac{RT}{F}\int \sum \frac{t_i^{\mathrm{IEM}}}{z_i} \mathrm{d}\ln\gamma_i \tag{8}$$

where E_{IEM} is the membrane potential. E_{Don}^{L} is the Donnan potential on the left side. E_{Don}^{R} is the Donnan potential on the right side. E_{diff} is the diffusion potential arising from the concentration gradient within the membrane and from the diffusivity difference of two ions. R is the universal gas constant. T is the absolute temperature. F is the faraday constant. t_i^{IEM} is the transport number in IEMs. z_i is the ion valence. γ_i is the ion activity.

Assuming that the ion transport number is usually constant [34], the simple expression for the membrane potential is [22, 32, 35]:

$$E_{\mathrm{AM/CM}} = \alpha_{\mathrm{AM/CM}} \frac{RT}{z_i F} \mathrm{In} \frac{\gamma_{\mathrm{AM/CM}}^{\mathrm{SOL,R}}}{\gamma_{\mathrm{AM/CM}}^{\mathrm{SOL,L}}} \tag{9}$$

$$E_{\mathrm{BM}} = \alpha_{\mathrm{BM}} \frac{RT}{z_i F} \mathrm{In} \frac{\gamma_{H^+} \gamma_{\mathrm{OH}^-}}{K_W} \tag{10}$$

where $E_{\mathrm{AM/CM}}$ and E_{BM} is the membrane potentials of AM/CM, and BPM, respectively. $\alpha_{\mathrm{AM/CM}}$ and α_{BM} is the apparent permselectivity of AM/CM and BPM, respectively. $\gamma_{\mathrm{AM/CM}}^{\mathrm{SOL,R}}$ is the ion activity in the solution at the right side of AM/CM. $\gamma_{\mathrm{AM/CM}}^{\mathrm{SOL,L}}$ is the ion activity in the solution at the left side of AM/CM. $\gamma_{H^+/\mathrm{OH}^-}$ is the H^+ or OH^- ion activity in the solution at both sides of BPM. K_W is the ion-product constant of water.

2.3. Ducts and slots resistance

Adjacent cell pairs are connected by the solutions passing across the slots and ducts within the EDBM stack. The slots and ducts act like a bridge for the electrolyte stream and unavailable electric current, as shown in Fig. 2. The resistance of the ducts and slots can be calculated depending on their geometric dimensions and the conductivity of the liquid flowing through them [15, 18, 36].The duct resistance can be defined as:

$$R_{\mathrm{ID}} = \frac{3h + h_{\mathrm{AM}} + h_{\mathrm{CM}} + h_{\mathrm{BM}}}{\Lambda_I A_D} \tag{11}$$

$$R_{\mathrm{OD}} = \frac{3h + h_{\mathrm{AM}} + h_{\mathrm{CM}} + h_{\mathrm{BM}}}{\Lambda_O A_D} \tag{12}$$

where R_{ID} and R_{OD} represents the resistance of the inlet and outlet ducts, respectively. h_{AM}, h_{CM}, and h_{BM} represents the thickness of the AM, CM, and BPM, respectively. Λ_I and Λ_O is the solution conductivity of the inlet and outlet ducts, respectively. A_D is the cross-sectional area of the ducts.

From each point in the compartment, there is an effective current perpendicular to the membranes through the cell pair, and small lateral ionic shortcut currents in the direction of the slots [18, 37, 38]. The slot resistance can be defined as:

$$R_{\mathrm{IS}} = \frac{l_S}{\Lambda_I b_S h} + R_L \tag{13}$$

$$R_{\mathrm{OS}} = \frac{l_S}{\Lambda_O b_S h} + R_L \tag{14}$$

where R_{IS} and R_{OS} represents the resistance of the inlet and outlet slots, respectively. l_S represents the length of the slots. b_S is the width of the slots. R_L represents the resistance of the lateral spacer, and can be determined by referring to references [18, 38].

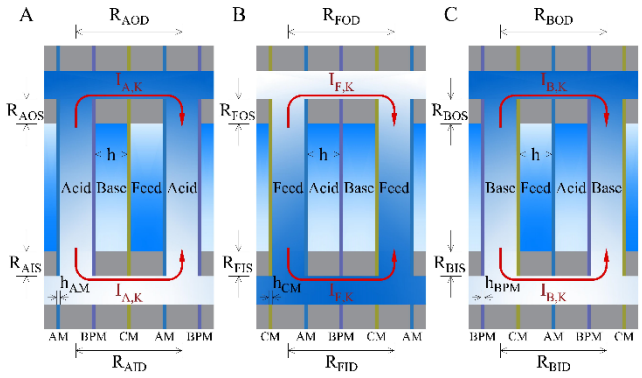

Fig. 2. Resistance schematic of the ducts and slots in the cell pair. A, B and C represents the ducts/slots in the acid, feed and base compartment respectively.

2.4. Leakage currents in external circuits

Three independent hydraulic circuits of a EDBM for producing an acid and base are considered in the equivalent circuit model. The model is formulated by means of converting the complex electrochemical processes into determined parameters, as shown in Fig. S5, which is consistent in principle with previous ED systems [17, 20, 39, 40]. The direct current, which branches as it passes through the membrane stack, is supplied to the electrical circuit network, and leakage currents from the external circuits occur at the ducts and slots. Although the concentration of the solution has a difference between the inlet duct (or slot) and the outlet duct (or slot) at the same position in the stack, the potential at the given position is identical due to an identical electrical resistance ratio. Hence, the equivalent circuit can be simplified by combining the inlet part with the outlet part and forming a simplified circuit shown in Fig. S6. The resistances R_{A}, R_{F}, R_{B}, and R_{CP} are defined as:

$$R_A = R_{\mathrm{AC}} + R_{\mathrm{AM}} \tag{15}$$

$$R_F = R_{\mathrm{FC}} + R_{\mathrm{CM}} \tag{16}$$

$$R_B = R_{\mathrm{BC}} + R_{\mathrm{BM}} \tag{17}$$

$$R_{\mathrm{CP}} = R_A + R_F + R_B \tag{18}$$

The membrane potential generated in the cell pair is defined as:

$$E_{\mathrm{CP}} = E_{\mathrm{AM}} + E_{\mathrm{CM}} + E_{\mathrm{BM}} \tag{19}$$

The shunt resistance R_D of the duct can be defined as:

$$R_D = \frac{R_{ID}R_{OD}}{R_{ID} + R_{OD}} \tag{20}$$

169 The shunt resistance R_S of the slot can be defined as:

$$R_S = \frac{R_{IS}R_{OS}}{R_{IS} + R_{OS}} \tag{21}$$

170 The shunt current L_K through the duct can be defined as:

$$L_K = l_{I,K} + l_{O,K} \tag{22}$$

171 The shunt current $J_{A,K}$ through the slot can be defined as:

$$J_K = j_{I,K} + j_{O,K} \tag{23}$$

172 Applying Kirchhoff laws to the equivalent circuit network of the *k*-th and the *k*+1-th cell as shown in Fig. 3, six

173 equations are derived from the electrical current balance equations:

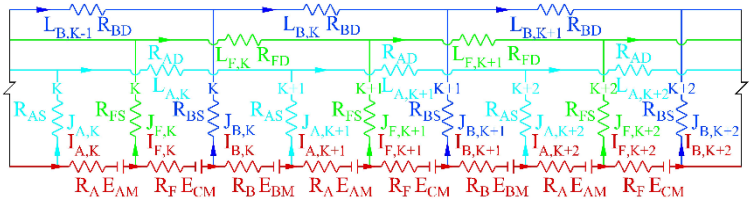

174

175 Fig. 3. Equivalent circuit network of the k-th and k+1-th cell in the BMED stack.

$$L_{A,K} + J_{A,K+1} = L_{A,K+1} \tag{24}$$

$$I_{B,K} = J_{A,K+1} + I_{A,K+1} \tag{25}$$

$$L_{F,K} + J_{F,K+1} = L_{F,K+1} \tag{26}$$

$$I_{A,K+1} = J_{F,K+1} + I_{F,K+1} \tag{27}$$

$$L_{B,K} + J_{B,K+1} = L_{B,K+1} \tag{28}$$

$$I_{F,K+1} = J_{B,K+1} + I_{B,K+1} \tag{29}$$

176 The potential balance equations for the *k*-th and *k*+1-th cell formed by the analog elements are:

$$J_{A,K}R_{AS} + L_{A,K}R_{AD} - J_{A,K+1}R_{AS} - I_{A,K}R_A - I_{F,K}R_F - I_{B,K}R_B - E_{CP} = 0 \tag{30}$$

$$J_{A,K+1}R_{AS} + L_{A,K+1}R_{AD} - J_{A,K+2}R_{AS} - I_{A,K+1}R_A - I_{F,K+1}R_F - I_{B,K+1}R_B - E_{CP} = 0 \tag{31}$$

$$J_{F,K}R_{FS} + L_{F,K}R_{FD} - J_{F,K+1}R_{FS} - I_{A,K+1}R_A - I_{B,K}R_B - I_{F,K}R_F - E_{CP} = 0 \tag{32}$$

$$J_{F,K+1}R_{FS} + L_{F,K+1}R_{FD} - J_{F,K+2}R_{FS} - I_{A,K+2}R_A - I_{B,K+1}R_B - I_{F,K+1}R_F - E_{CP} = 0 \tag{33}$$

$$J_{B,K}R_{BS} + L_{B,K}R_{BD} - J_{B,K+1}R_{BS} - I_{F,K+1}R_F - I_{A,K+1}R_A - I_{B,K}R_B - E_{CP} = 0 \tag{34}$$

$$J_{B,K+1}R_{BS} + L_{B,K+1}R_{BD} - J_{B,K+2}R_{BS} - I_{F,K+2}R_F - I_{A,K+2}R_A - I_{B,K+1}R_B - E_{CP} = 0 \tag{35}$$

177 Due to the physical dimension of the slots is much less than the compartments, the electric resistance of the

178 slots is much larger than the compartments. Taking account of equations $R_{AS} \gg R_A$,$R_{AS} \gg R_B$,$R_{AS} \gg R_A + R_F$,R_{AS}

$\gg R_F + R_B$, differential calculus is used to determine the general solutions of the leakage currents $J_{A,K}$, $J_{F,K}$ and $J_{B,K}$ as shown in Appendix B. The electrical current $J_{A,1}$, $J_{F,1}$, $J_{B,1}$, $J_{A,2}$, $J_{F,2}$ and $J_{B,2}$ is determined as shown in Appendix C.

$$J_{A,K} = \frac{1}{\alpha_A - \beta_A}\left[\alpha^{k-1}_{A}(J_{A,2} - \beta_A J_{A,1}) - \beta^{k-1}_{A}(J_{A,2} - \alpha_A J_{A,1})\right] \quad (36)$$

$$J_{F,K} = \frac{1}{\alpha_F - \beta_F}\left[\alpha^{k-1}_{F}(J_{F,2} - \beta_F J_{F,1}) - \beta^{k-1}_{F}(J_{F,2} - \alpha_F J_{F,1})\right] \quad (37)$$

$$J_{B,K} = \frac{1}{\alpha_B - \beta_B}\left[\alpha^{k-1}_{B}(J_{B,2} - \beta_B J_{B,1}) - \beta^{k-1}_{B}(J_{B,2} - \alpha_B J_{B,1})\right] \quad (38)$$

$$[j_{A,1}, j_{F,1}, j_{B,1}]^T = A^{-1} b \quad (39)$$

$$[j_{A,2}, j_{F,2}, j_{B,2}]^T = \left[\frac{(\alpha^{N-2}_{A} - \beta^{N-2}_{A}) - (\alpha_A - \beta_A)}{\alpha^{N-1}_{A} - \beta^{N-1}_{A}} j_{A,1}, \frac{(\alpha^{N-2}_{F} - \beta^{N-2}_{F}) - (\alpha_F - \beta_F)}{\alpha^{N-1}_{F} - \beta^{N-1}_{F}} j_{F,1}, \frac{(\alpha^{N-2}_{B} - \beta^{N-2}_{B}) - (\alpha_B - \beta_B)}{\alpha^{N-1}_{B} - \beta^{N-1}_{B}} j_{B,1}\right]^T \quad (40)$$

By regrouping equations (23), (25), and (27), the general solutions of the leakage currents $L_{A,K}$, $L_{F,K}$, and $L_{B,K}$ are determined as shown in Appendix D.

$$L_{A,K} = \sum_{1}^{N-1} J_{A,K} \quad (41)$$

$$L_{F,K} = \sum_{1}^{N-1} J_{F,K} \quad (42)$$

$$L_{B,K} = \sum_{1}^{N-1} J_{B,K} \quad (43)$$

2.5. Joule heating effect in the external circuit

Leakage currents can cause undesirable heat and may even affect non-metallic components used in the stack. Although leakage currents are not high compared to the input current of the stack, the Joule heating effect in the external circuit may be high due to the high resistance of the ducts and slots. Meanwhile, these ducts and slots act mainly as liquid bridges, distribute untreated solutions, and then converge the treated solutions. When the liquids flow through the ducts and slots, the undesired heat generated there can be taken away. Because the space is so small, the aggregation of heat may occur there, as shown in Fig. 4. The thermal effects of the ducts and slots can be determined by assuming the resistive heating due to leakage currents contribute directly to raising the local temperature of the fluid (details provided in Appendix E), the temperature rise is calculated to be,

$$\Delta T_K^D = \frac{L_K^2 R_D}{C\rho Q_D} \tag{44}$$

$$\Delta T_K^S = \frac{J_K^2 R_S}{C\rho Q_S} \tag{45}$$

where ΔT_K^D and ΔT_K^S is the rising temperatures of the ducts and slots, respectively. C is the specific heat capacity of the liquid through the ducts and slots in each compartment. ρ is the density of the liquid through the ducts and slots. Q_D and Q_S is the flow rate of the liquid through the ducts and slots, respectively.

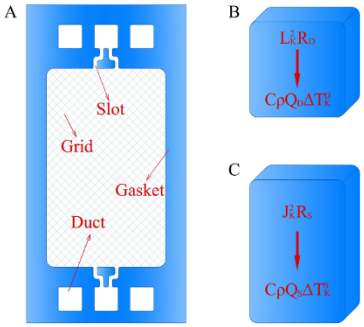

Fig. 4. Joule heating effect at the ducts and slots. A. Spacer. B. Duct. C. Slot.

3. Experiment

Three sets of tests were conducted in our work. Lab-scale tests and software simulation tests were to validate the model, and the pilot tests were to explain these effects in a magnified stack.

Lab-scale experiment - The EDBM apparatus used in this study is the same as the one used in our previous research [21]. To maintain the same concentration of feed into each compartment in each feed-and-bleed process, single-pass circulating hydraulic circuit where the acid stream, the feed stream, and the base stream outputs from the membrane stack mixed in a supply tank, and returned into each compartment. The module of the membrane stack was composed of five cell pairs with a full-format membrane, of 100 mm × 300 mm. The spacers and IEM properties are shown in Table 1 and 2. Three batches of experiments were set up, and solution details were shown in Table 3. The solution in each compartment flowed at a rate of 5 cm.s^{-1} in a parallel flow during the whole process. When the solution had circulated in each compartment for 5 min, a stabilized current density of 30 mA.cm^{-2} was applied to the membrane stack. Platinum wires were inserted into the slots of all the compartments at cell-pairs one, three, and five, to measure voltages. Meanwhile, the leakage currents through the slots are equal to the voltage applied to the slots divided by its resistance.

Table 1 Spacer properties in the lab-scale test.

Items	Unit	Value
Gasket		
Thickness	mm	1.2

Effective area	cm	21×7
Ducts	mm	14×12
Slots	mm	28×1.4
Spacer porosity		
Filament diameter	mm	0.3
Filament pitch	mm	2.7
Porosity	%	86.1
Shadow effect (max)	%	36.5 (38)

212 Table 2 IEMs properties in the lab-scale test.

Items	Unit	Value
CGU		
Manufacturer	Tokuyama Soda Co. Japan	
Thickness	mm	0.22
Resistance	Ω.cm²	2.0
AHA		
Manufacturer	Tokuyama Soda Co. Japan	
Thickness	mm	0.22
Resistance	Ω.cm²	4.1
FBM		
Manufacturer	Fuma.Tech GmbH, Germany	
Thickness	mm	0.20
Resistance	Ω.cm²	3.0

The conductivity of the membranes was determined in a 0.5 M NaCI solutions at 25 ℃.

213 Table 3 Details of the three batches experiments.

Exp.	Supply tank		Electrode tank	
	C_{NaCl}	V_{NaCl}	C_{Na2SO4}	V_{Na2SO4}
1	0.3 M	2 L	0.5 M	2 L
2	0.5 M	2 L	0.5 M	2 L
3	0.8 M	2 L	0.5 M	2 L

214 Simulation experiment - The electrical network of EDBM stack was analyzed by Multisim software version
215 14.0 (American Instrument Company, USA). Firstly, the equivalent circuit of EDBM stack were input to
216 Workspace Panels in Multisim. Secondly, the resistances, current and potential values in the equivalent circuits
217 were imported. Finally, the leakage currents through the slots of each circuit in the stack were solved.

218 Pilot-scale experiment - 40 L of carbocysteine wastewater was circulated through the feed compartment, and
219 120 L of dilute HCl (Cond. 40 $mS.cm^{-1}$) and 100 L of dilute NH_4OH/NH_4Cl (Cond. 12 $mS.cm^{-1}$) were circulated
220 through the acid and base compartments respectively, driven by different pumps at a constant flow rate of 5 $cm.s^{-1}$
221 in the EDBM system with three-compartment. The module of the membrane stack was composed of 25 (or 45)
222 cell pairs with a full-format membrane, of 560 mm × 310 mm. The spacers and IEM properties are shown in Table
223 4. When the solution had circulated in each compartment for 10 min, a stabilized current density of 50 $mA.cm^{-2}$
224 was applied to the membrane stack. During the EDBM process, the solution conductivity in each compartment
225 was measured by a conductometer (WTW Cond 330i, Xylem Analytics Germany GmbH, Germany) at 20 min
226 intervals.

227 Table 4 Parameters corresponding to the pilot-scale test.

Items	Units	Value
Cell number	pair	25
Flow rate	$cm.s^{-1}$	5
Current density	$mA.cm^{-2}$	50
FAB		
Thickness	mm	0.12
Resistance	Ω.cm²	1.0
FKB		
Thickness	mm	0.1
Resistance	Ω.cm²	4.0
FBM		
Thickness	mm	0.2
Resistance	Ω.cm²	3.0
Spacer Gasket		
Thickness	mm	1.2
Effective area	cm	30×20
Ducts	mm	14×14
Slots	mm	28×1.4
Spacer Porosity		
Filament diameter	mm	0.3
Filament pitch	mm	3.0
Porosity	%	86.5
Shadow effect	%	63.3

All IEMs were purchased from Fuma.Tech GmbH, Germany.

4. Results and Validation

The resistance of each cell pair was determined by using the cell pair resistance model. The experimental measured results and the calculated values from the cell pair resistance model are plotted in Fig. 5. The resistances of a cell pair predicted by the cell pair resistance model approximated to the experimental results, as shown in Table 5. The maximum deviation (8.2%) occurred due to an underestimation of the IEM's resistance in the 0.3 M NaCl solution, however this effect can be minimized by using the resistance model of the membranes. Although a deviation existed between the model and the experimental results, the cell pair resistance model is still valid owing to the small absolute values [41]. The results of leakage currents through the slots from the software simulated and the model calculated are plotted in Fig. 6. The deviation between the model values and the simulation results is less than 0.2%, and the average deviation is approximately 0.12% (0.3 M NaCl), 0.06% (0.5 M NaCl), and 0.09% (0.8 M NaCl). The model and simulation results are consistent, which shows that the application of the differential calculus method is valid. The results of leakage currents through the slots from the experimental measured and the model calculated are plotted in Fig. 7.The deviation of leakage currents through the slots between the model and the experimental results are all less than 10%, and the average deviation is

approximately 7.5% (0.3 M NaCl), 3.1% (0.5 M NaCl), and 4.8% (0.8 M NaCl). Although there existed a small deviation, it is acceptable owing to the small absolute values of the leakage currents (the ratio of leakage current and total current is less than 0.1%) [41]. Hence, the mathematical model can be applied for the assessment of the leakage currents in the external circuit in the EDBM stack.

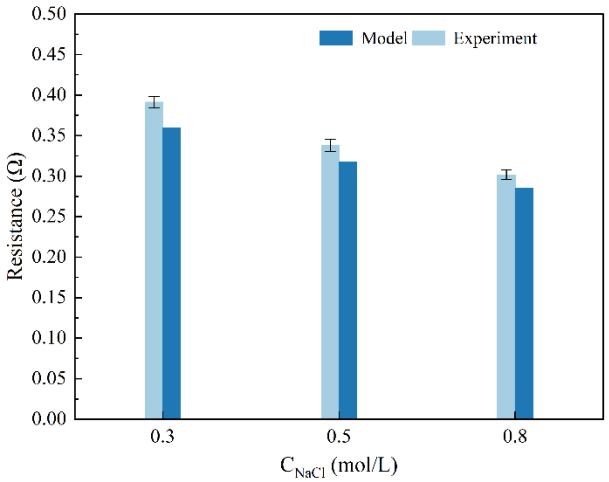

Fig. 5. Comparison of model-predicted cell pair resistances against experimental measurements.

Table 5 Comparison of model-predicted cell pair resistances against experimental measurements.

Solution	$R_{Cell\ pair}$ (Ω)		Deviation
NaCl	Model	Experiment	
0.3 M	0.36	0.39	8.2%
0.5 M	0.32	0.34	6.2%
0.8 M	0.29	0.30	6.4%

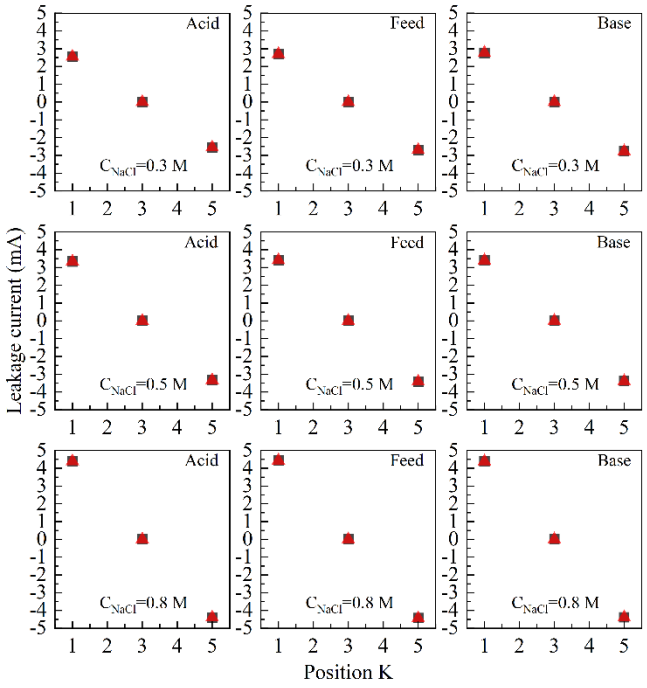

Fig. 6. Comparison of leakage currents through the slots predicted by our model with simulation results. Each graph shows the experimental results (triangle) and model values (Square).

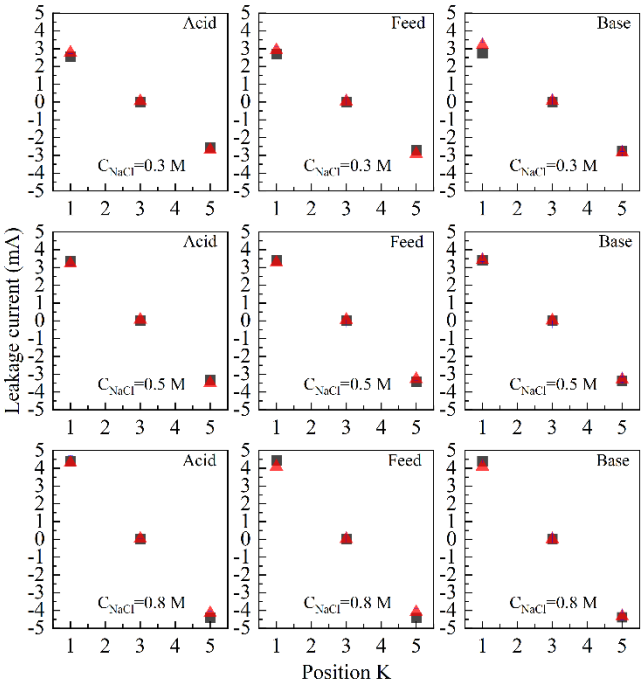

Fig. 7. Comparison of leakage currents through the slots predicted by our model with experimental results. Each graph shows the experimental results (Square) and model values (triangle). Error bars, represent standard deviation in voltage measurements, not visible are smaller than the symbol size.

5. Discussion

Leakage currents in the external circuit are a function of their position, cell pair number, current density, and element resistivity according to the leakage currents equation. Leakage currents not only cause loss of coulombic efficiency but also create undesirable Joule heat, especially during the termination stage. This section presents a summary of a systematic study on the distribution and influencing factors of the leakage currents, and the Joule heating effect in the external circuit. Numerical values of a baseline case considered in this study are shown in Table 4.

5.1. Distribution of the leakage currents

The leakage currents model indicates that its value is related to the position of the liquid bridges in the stack. The distribution of leakage currents in the stack is shown in Fig. 8. Leakage currents through the slots are highest in the outermost cells and they change sign in the central portion of the stack, as is shown in the distribution of the points in Fig.

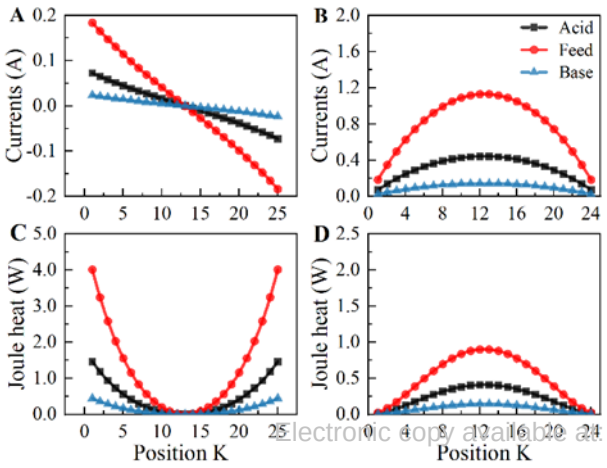

8A. Leakage currents through the ducts are highest at or near the center of the cells and they keep the same sign in all positions of the stack, as is shown in the distribution of the points in Fig. 8B. The underlying reason for this observation was explained in our previous literature [21]. It should be noted that the leakage currents and Joule heat both increase as the resistance decreases. Based on Joule's law, the Joule heat at the slots or the ducts is proportional to the square of the currents within the given state. Hence, the Joule heat of the slots near the outermost cell pair and the ducts near the center of the cell pairs is highest, as is evident from Figs. 8C, and D, and these positions in the stack should be focused on.

Fig. 8. Leakage currents and Joule heat through or at the slots and ducts against the membrane pair position. A. Leakage currents through slots. B. Leakage currents through ducts. C. Joule heat at slots. D. Joule heat at ducts. Numerical values of a baseline case from the pilot-scale test were presented in Table 4. On a given moment, the conductivity of the bulk stream is 40.4 $mS \cdot cm^{-1}$, 119.6 $mS \cdot cm^{-1}$, 11.87 $mS \cdot cm^{-1}$ in the acid, feed and base compartment respectively.

5.2. Effect of the cell pair number

A EDBM stack contains from a few cells up to several hundred of cells and two electrode compartments [14, 33], which allows the current of ions to be converted into a current of electrons flowing through an external electrical circuit. Based on the model, the leakage currents are a function of the cell number. The parameters were substituted into the model of the leakage currents, and the results are shown in Figs. 9. From Figs. 9A, B and C, the cell number can be seen to have a significant influence on the leakage currents through the slots near the outermost cells, but a small influence on the leakage currents through the slots near the central cells. Similarly, the cell number has a small influence on the leakage currents through the ducts near the outermost cells, but a significant influence on the leakage currents through the ducts near the central cells, as shown in Figs. 9D, E and F. Moreover, the degree of desalination, the price of the electrode, and the power consumption should be considered in industrial EDBM stack installations, resulting in as many cells as possible, and only limited by the available space[18, 40, 42]. In a large EDBM stack, the leakage currents through the slots near the outermost cells and the ducts near the central cells should be considered seriously, as is evident from Fig. 8 and Fig. S7. From Fig. 9G and H, the leakage currents through the slots at the outermost cells and the ducts near the central cells increase steeply with a small increase in the cell number, and reach a maximum after a certain number of cell pairs. Note that the input current was kept constant. Thus, to maintain current output as the cell number increase, extra current must be generated to compensate for the increase leak to the external circuits, and leakage current would saturate when leakage currents ratio reached the threshold of the stack[37]. Although the leakage currents are maximized at the 'saturation effect' stage, the number of cell pairs should be chosen based on economics. Meanwhile, some measures, such as decreasing the current density or increasing the resistance of the slots and ducts, can offset this effect in a large stack.

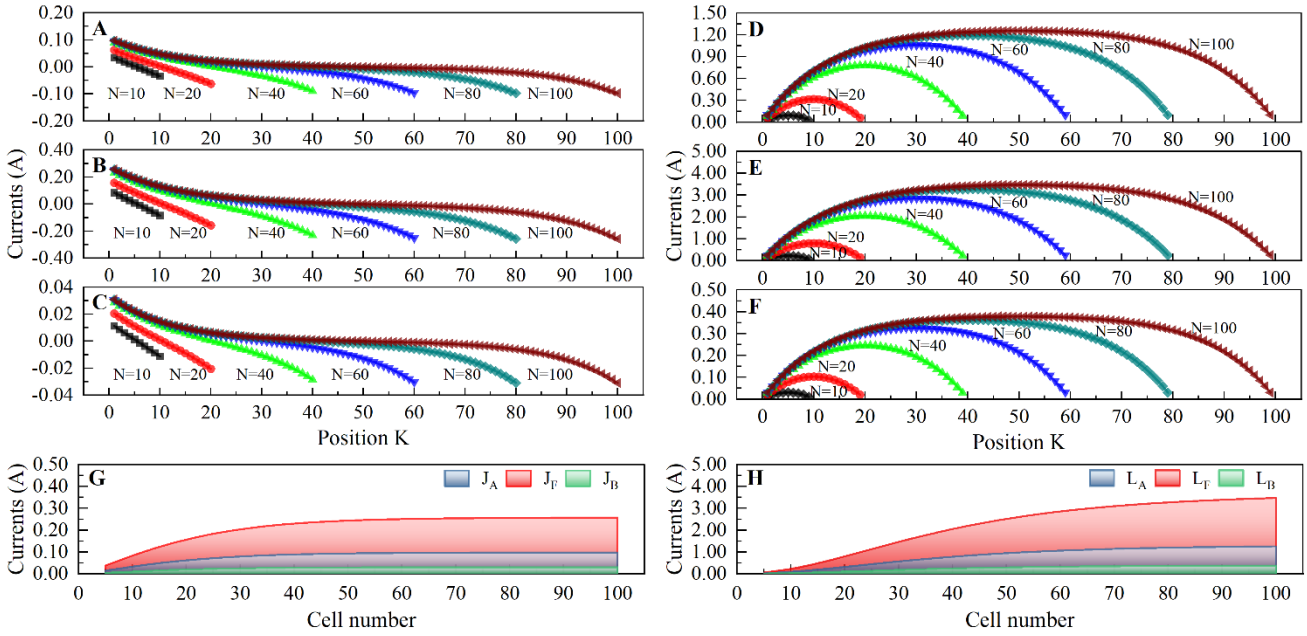

Fig. 9. Leakage currents flowed through the slots and ducts against the cell number. The conductivity of the bulk stream is the same as section 5.1, and the other parameters was listed in Table 4. A, B and C represents the currents through the slots in the acid, feed and base compartment respectively. D, E and F represents the currents through the ducts in the acid, feed and base compartment respectively. G represents the currents through the slots at the outermost cells against the cell number, and J_A, J_F and J_B represents the currents through the slots in the acid, feed and base compartment respectively. H represents the currents through the ducts at or near the central of the cells against the cell number, and L_A, L_F and L_B represents the currents through the ducts in the acid, feed and base compartment respectively.

5.3. Effect of the current density

Limiting current density has been deemed to be a practical upper threshold for common ED/EDBM operations [43, 44]. The applicable range of current density is 50 to 150 $mA \cdot cm^{-2}$ in practical operations for EDBM technology [4]. Commonly, enhancing the current density can reduce the membrane area requirements, resulting in lower total costs [45]. Moreover, overlimiting current density operation has been tested at a laboratory scale and shows enhanced mass transfer [46], meaning that a higher current density can be applied for efficient ED/EDBM systems. The variation of current density thus has an effect on leakage currents as depicted in Fig. 10. As the current density increases, the leakage currents through the slots near the outermost cells (K = 1–40, or K = 461–500) increase markedly, and the rate of increase is higher at points closest to the outermost cells, as is evident from Fig. 10A, B and C. From Fig. 10D, E and F, the leakage currents through the ducts at all positions have been affected by the current density, and the rate of increase reached a maximum at the 'saturation effect' stage ($K \geq 40$ or $K \leq 461$). That is to say, increasing the current density increase the leakage current through the external circuits. The main reason is that increasing the current density causes an increase in the potential difference, and

then drives a higher leakage current. Hence, an appropriate current density should be chosen before the Joule heating effect at the slots and ducts is assessed. Generally, different current densities were applied for a multi-stage EDBM processing, resulting in a decreased Joule heating effect at the slots, as shown in Fig. S7.

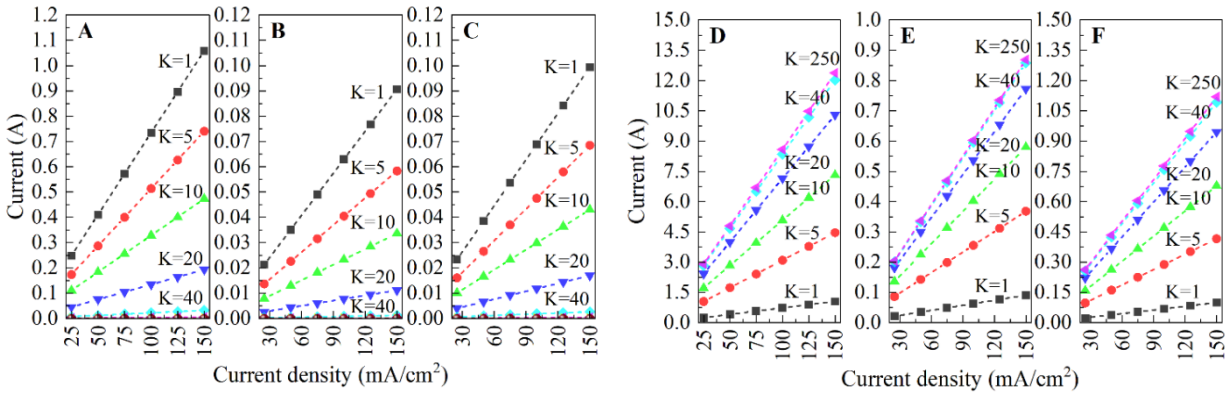

Fig. 10. Leakage currents flowed through the slots in the k-th cell against the current density. These results are symmetric about K = 250. The number of cell pairs is 500, the conductivity of the bulk stream is 144.4 mS·cm^{-1}, 9.03 mS·cm^{-1}, 11.74 mS·cm^{-1} in the acid, feed and base compartment respectively, and the other parameters was listed in Table 4. A, B and C represents the currents through the slots in the acid, feed and base compartment respectively. D, E and F represents the currents through the ducts in the acid, feed and base compartment respectively.

5.4. Effect of R_S/R_{CP} and R_D/R_{CP}

The model of leakage currents indicates that the leakage currents are affected by the resistance of the slots, ducts, and cell pairs. The varying resistance ratios (R_S/R_{CP} = 1957, 978, 489, 326, 245 and R_D/R_{CP} = 27, 15, 10, 7,5) were set up with other parameters as shown in Table 4 except that the number of cell pairs was 100. The effect of the resistance ratios on the leakage currents are plotted in Fig. 11. Leakage currents through the slots at the outermost cells (as well as the other positions except for the central cell pair) were affected by both resistance ratios. Moreover, the leakage currents increased faster as the resistance ratios decreased, as shown by the contour line density in Fig. 11A. Similarly, leakage currents through the ducts at every position were mainly dominated by the resistance ratio of R_D/R_{CP} in Fig. 11B. The leakage currents increased faster as the resistance ratio of R_D/R_{CP} decreased. These results indicate that the resistance ratios, R_S/R_{CP} and R_D/R_{CP} should be as high as possible at the stacks. In fact, R_S/R_{CP} and R_D/R_{CP} depend on the size of the slots, the ducts, the spacers, the thickness of the spacers, the conductivity of the solutions, and the concentration polarization. For this reason, the size of the slots and ducts should be as small as possible, and the active area of the spacers should be large. However, a small size slot and duct and a thin spacer would increase pressure drops, and a large area spacer would affect the distribution of flow rates, resulting in increasing the energy consumption [14]. The leakage currents model indicated the need for choosing an appropriate spacer. During the later stages of the EDBM process, the low conductivity of solutions

in some compartments increases the resistance of cell pairs [8], increasing the leakage currents, especially when concentration polarization occurred. Therefore, it is important to consider an appropriate endpoint during EDBM process.

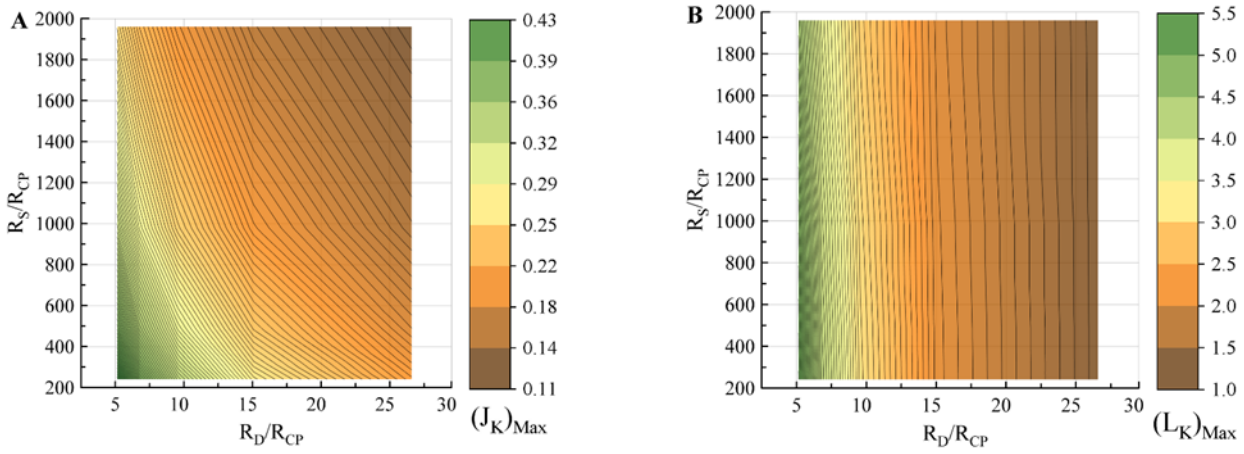

Fig. 11. Leakage currents flowed through the slots in the outermost cells and the ducts near the central cells against R_S/R_{CP} and R_D/R_{CP}. The conductivity of each compartment is 84.0 $mS \cdot cm^{-1}$, and the leakage currents of each compartment is almost the same. A. Slots. B. Ducts.

5.5. Joule heating effect of the external circuit

Leakage currents not only lead to losses of electrical coulombic efficiency [15], but may also affect the safety of the device. The overheating phenomenon often occurred at the end of desalination, especially when a weak electrolyte was used [8, 21]. The parameters were acquired from the pilot-scale test, and the Joule heating effect in the external circuit is plotted against the membrane pair position at the end of desalination and is shown in Fig. 12. The Joule and temperature effect ΔT at the slots in the outermost cell was significant and gradually decreased from the outermost cell to the central cell. Conversely, the Joule heating effect and temperature effect ΔT at the ducts near the central cell were significant and gradually decreased from the central cell to the outermost cell. Moreover, the Joule heating effect and temperature effect ΔT in the external circuit in the acid compartment greatly exceeded that in the other compartments because the conductivity of the acid solution is significantly better than the solution in the other compartments. The maximum value of the Joule heating effect at the slots was 1.64 times as much as at the ducts in the acid compartment. The maximum value of the temperature effect ΔT at the slots (increased by 12.18 ℃ in about 0.3 s) was significantly higher than at the ducts (increased by 0.08 ℃ in about 0.3 s). The main reason for this is that the slots are smaller in size than the ducts, and the flux of the solution through the ducts is N (cell pairs number) times as much as the slots. Hence, the conductivity and flux of solutions should be considered in a big stack, especially at the end of desalination.

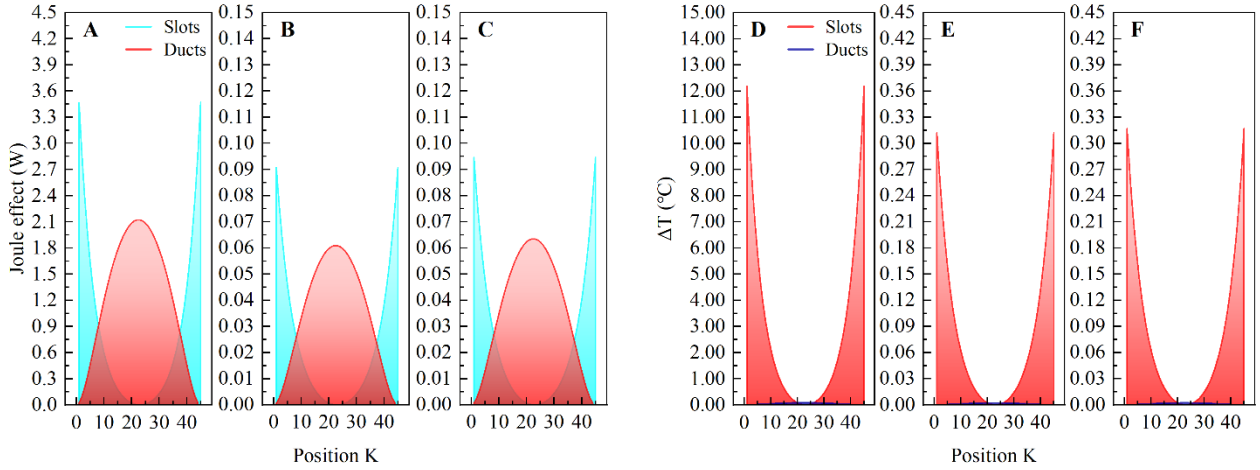

Fig. 12. Joule heating effect at the external circuit against the membrane pair position at the end of desalination. The number of cell pairs is 45, the conductivity of the bulk stream is 288.50 mS·cm^{-1}, 6.72 mS·cm^{-1}, 6.33 mS·cm^{-1} in the acid, feed and base compartment respectively, and the other parameters was listed in Table 4. A and D. Acid. B and E. Feed. C and F. Base.

6. Conclusions

Mathematical models for cell pair electrical analog and leakage currents in a EDBM stack used for producing an acid and base are proposed and validated using both experiments and simulations. Based on the characteristic of a network circuit, leakage currents through the external circuit in each compartment presented a symmetrical distribution. Leakage currents were highest through the slots at the outermost cell and the ducts near the central cell. Meanwhile, leakage currents and Joule heat both increase as the resistance decreases. Leakage currents in a EDBM stack are sensitive to the number of cell pairs, current density, the resistance ratio of the slot and cell pair $R_S/R_{CP,}$ and the resistance ratio of the duct and cell pair R_D/R_{CP}. Leakage currents increase as the number of cell pairs (or current density) increase. The two resistance ratios can reflect the geometric characteristics of the spacers and should be as high as possible at the stacks, to reduce the leakage current. The Joule heating effect in the external circuit may affect the non-metallic spacers. The Joule heat generated at the slots in the outermost cell is more significant than at the ducts in the central cell. The temperature effect is more pronounced as the solution conductivity increases, or the flux decreases. These findings will help to assess the leakage currents when designing EDBM stack so they can be minimized for when the system is built.

Acknowledgements

The financial support from National Natural Science Foundation of China (51578131) are greatly appreciated. We also thank the anonymous reviewers for their very valuable comments to improve this work.

Nomenclature

R_C	Resistance of the bulk stream in each compartment, Ω.
$\overline{\Lambda}$	Average conductivity of the bulk stream except for DBLs, $S \cdot m^{-1}$.
$\overline{\Lambda^{DBL}}$	Average conductivity of the bulk stream in DBLs, $S \cdot m^{-1}$.
h	Thickness of each compartment, m.
A	Effective area of membranes, m^2.
D	Diffusion coefficient of the electrolyte in the solutions, $cm^2 \cdot s^{-1}$.
d_f	Filament diameter in the spacer, m.
l_f	Filament pitch in the spacer, m.
$R_{AM/CM}$	Resistance of the AM or CM, Ω.
R_{BPM}	Resistance of the BPM, Ω.
f	Shadow factor or shadow effect, %.
$\Lambda_{I/II}$	Conductance resulting from the ions in the microcavities or microchannels, $S \cdot m^{-2}$.
C	Concentration of ions, $mol \cdot L^{-1}$.
x	Position in the membrane, m.
n	Fit parameter.
r_{AEL}	Resistance of the AEL, $\Omega \cdot m^2$.
r_{CEL}	Resistance of the CEL, $\Omega \cdot m^2$.
r_{IL}	Resistance of the IL, $\Omega \cdot m^2$.
Λ_{H^+/OH^-}	Conductivity of the H^+ or OH^- ion, $S \cdot m^{-2} \cdot mol^{-1}$.
E_{IEM}	Membrane potential, V
E_{Don}^{L}	Donnan potential on the left side, V.
E_{Don}^{R}	Donnan potential on the right side, V.
E_{diff}	Diffusion potential, V.
R	Universal gas constant, $8.3145\ J \cdot mol^{-1} \cdot K^{-1}$.
T	Absolute temperature, K.

F	Faraday constant, 9.6485×10^4 C·mol^{-1}.
t_i^{IEM}	Transport number in the IEMs.
z_i	Ion valence.
K_W	Ion constant of water.
R_{ID}	Resistance of the inlet ducts in each compartment, Ω.
R_{OD}	Resistance of the outlet ducts in each compartment, Ω.
h_{AM}	Thickness of the AM, m.
h_{CM}	Thickness of the CM, m.
h_{BPM}	Thickness of the BPM, m.
Λ_I	Solution conductivity of the inlet ducts/slots in each compartment, S·m^{-1}.
Λ_O	Solution conductivity of the outlet ducts/slots in each compartment, S·m^{-1}.
A_D	Cross-sectional area of the ducts in the spacer, m^2.
R_{IS}	Resistance of the inlet slots in each compartment, Ω.
R_{OS}	Resistance of the outlet slots in each compartment, Ω.
R_L	Resistance of the lateral spacer resistance in each compartment, Ω.
l_S	Length of the slots in the spacer, m.
b_S	Width of the slots in the spacer, m.
I_{K}	Cell current through the *k*-th cell in each compartment, A.
$l_{\mathrm{I,K}}$	Current through the inlet ducts in each compartment, A.

$l_{O,K}$	Current through the outlet ducts in each compartment, A.
$j_{I,K}$	Current through the inlet slots in each compartment, A.
$j_{O,K}$	Current through the outlet slots in each compartment, A.
N	Cell number in the stack.
K	Position of cell pair in the stack.
R_A	Resistance of the acid compartment and the AM, Ω.
R_F	Resistance of the feed compartment and the CM, Ω.
R_B	Resistance of the base compartment and the BPM, Ω.
R_{CP}	Resistance of cell pair, Ω.
E_{CP}	Membrane potentials generated in the cell pair, V.
R_D	Shunt resistance of the inlet and outlet ducts in each compartment, Ω.
R_S	Shunt resistance of the inlet and outlet slots in each compartment, Ω.
$L_{A,K}$	Shunt current through the inlet and outlet ducts in the acid compartment, A.
$L_{F,K}$	Shunt current through the inlet and outlet ducts in the feed compartment, A.
$L_{B,K}$	Shunt current through the inlet and outlet ducts in the base compartment, A.
$J_{A,K}$	Shunt current through the inlet and outlet slots in the acid compartment, A.

$J_{F,K}$ Shunt current through the inlet and outlet slots in the feed compartment, A.

$J_{B,K}$ Shunt current through the inlet and outlet slots in the base compartment, A.

A^{-1} Inverse matrix.

ΔT_K^D Rising temperatures of the inlet or outlet ducts in each compartment, ℃.

ΔT_K^S Rising temperatures of the inlet or outlet slots in each compartment, ℃.

C specific heat capacity of the liquid through the ducts/slots in each compartment, $J \cdot kg^{-1} \cdot ℃^{-1}$.

Q Flow rate of the liquid, $L.S^{-1}$.

Greek symbols

σ Thickness of DBLs, m.

ε Porosity of the spacer.

δ Thickness of the membranes, m.

λ Thickness of the IL, m.

u Mobility of the ions, $m^2 \cdot s^{-1} \cdot v^{-1}$.

γ_i Ion activity.

$\alpha_{AM/CM/BM}$ Membrane permselectivity.

α, β Solutions of equation $X^2-2(1+\Delta_A)X+1=0$.

ρ Density of the stream, $kg \cdot m^3$.

References

[1] M. Poliakoff, J.M. Fitzpatrick, T.R. Farren, P.T. Anastas, Green chemistry: science and politics of change, Science 297 (2002) 807-810.

[2] M.A. Shehzad, A. Yasmin, X. Ge, Z. Ge, K. Zhang, X. Liang, J. Zhang, G. Li, X. Xiao, B. Jiang, L. Wu, T. Xu, Shielded goethite catalyst that enables fast water dissociation in bipolar membranes, Nature Communications 12 (2021) 9. https://doi.org/10.1038/s41467-020-20131-1.

[3] S. Chabi, K.M. Papadantonakis, N.S. Lewis, M.S. Freund, Membranes for artificial photosynthesis, Energy & Environmental Science 10 (2017) 1320-1338. https://doi.org/10.1039/C7EE00294G.

[4] K. Mani, Electrodialysis water splitting technology, Journal of membrane science 58 (1991) 117-138. https://doi.org/10.1016/S0376-7388(00)82450-3.

[5] S.Z. Oener, M.J. Foster, S.W. Boettcher, Accelerating water dissociation in bipolar membranes and for electrocatalysis, Science 369 (2020) 1099-1103. https://doi.org/10.1126/science.aaz1487.

[6] N.A. Kelly, 6 - Hydrogen production by water electrolysis, in: A. Basile, A. Iulianelli, Advances in hydrogen production, storage and distribution, Woodhead Publishing2014, pp. 159-185. https://doi.org/10.1533/9780857097736.2.159.

[7] M. V. Guzman, P. Guedes, N. Couto, L.M. Ottosen, A.B. Ribeiro, J.M. Rodriguez-Maroto, Electrodialytic phosphorus recovery from sewage sludge ash under kinetic control, Electrochim Acta 287 (2018) 49-59. https://doi.org/10.1016/j.electacta.2018.08.032.

[8] Y. Li, S. Shi, H. Cao, X. Wu, Z. Zhao, L. Wang, Bipolar membrane electrodialysis for generation of hydrochloric acid and ammonia from simulated ammonium chloride wastewater, Water Research 89 (2016) 201-9. https://doi.org/10.1016/j.watres.2015.11.038.

[9] R. Ibáñez, A. P. González, P. Gómez, A.M. Urtiaga, I. Ortiz, Acid and base recovery from softened reverse osmosis (RO) brines. Experimental assessment using model concentrates, Desalination 309 (2013) 165-170. https://doi.org/10.1016/j.desal.2012.10.006.

[10] E. Rozoy, L. Boudesocque, L. Bazinet, Deacidification of cranberry juice by electrodialysis with bipolar membranes, Journal of agricultural and food chemistry 63 (2015) 642-651. https://doi.org/10.1021/jf502824f.

[11] A. Grabowski, G. Zhang, H. Strathmann, G. Eigenberger, The production of high purity water by continuous electrodeionization with bipolar membranes: influence of the anion-exchange membrane permselectivity, Journal of Membrane Science 281 (2006) 297-306. https://doi.org/10.1016/j.memsci.2006.03.044.

[12] L. Shi, Y. Hu, S. Xie, G. Wu, Z. Hu, X. Zhan, Recovery of nutrients and volatile fatty acids from pig manure hydrolysate using two-stage bipolar membrane electrodialysis, Chemical Engineering Journal 334 (2018) 134-142. https://doi.org/10.1016/j.cej.2017.10.010.

[13] C. Huang, T. Xu, Electrodialysis with bipolar membranes for sustainable development, Environmental Science & Technology 40 (2006) 5233-43. https://doi.org/10.1021/es060039p.

[14] A. Campione, L. Gurreri, M. Ciofalo, G. Micale, A. Tamburini, A. Cipollina, Electrodialysis for water desalination: A critical assessment of recent developments on process fundamentals, models and applications, Desalination 434 (2018) 121-160. https://doi.org/10.1016/j.desal.2017.12.044.

[15] T. Wen, G.S. Solt, D.W. Gao, Electrical resistance and coulomb efficiency of electrodialysis (ED) apparatus in polarization, Journal of Membrane Science 114 (1996) 255-262. https://doi.org/10.1016/0376-7388(96)00005-1.

[16] J.R. Wilson, Demineralization by electrodialysis, Butterworths Scientific Publications (1960).

[17] W. Mandersloot, R. Hicks, Leakage currents in electrodialytic desalting and brine production, Desalination 1 (1966) 178-193. https://doi.org/10.1016/S0011-9164(00)84017-5.

[18] J. Veerman, J.W. Post, M. Saakes, S.J. Metz, G.J. Harmsen, Reducing power losses caused by ionic shortcut currents in reverse electrodialysis stacks by a validated model, Journal of Membrane Science 310 (2008) 418-430. https://doi.org/10.1016/j.memsci.2007.11.032.

[19] M. Doležel, K. Keslerová, Measurement of non-effective electric current in electrodialysis stacks, Journal of The Electrochemical Society 164 (2017) 276-282. https://doi.org/10.1149/2.1481709jes.

[20] G. Belfort, G.A. Guter, An electrical analogue for electrodialysis, Desalination 5 (1968) 267-291. https://doi.org/10.1016/S0011-9164(00)80104-6.

[21] Z. Peng, Y. Sun, Leakage circuit characteristics of a bipolar membrane electrodialyzer with 5 BP-A-C units, Journal of Membrane Science 597 (2020) 117762. https://doi.org/10.1016/j.memsci.2019.117762.

[22] P. Ramirez, S. Mafe, J.A. Manzanares, J. Pellicer, Membrane potential of bipolar membranes, Journal of The Electrochemical Society 404 (1996) 187-193. https://doi.org/10.1016/0022-0728(95)04378-0.

[23] J.W. Post, H.V. Hamelers, C.J. Buisman, Energy recovery from controlled mixing salt and fresh water with a reverse electrodialysis system, Environmental science & technology 42 (2008) 5785-5790. https://doi.org/10.1021/es8004317.

[24] N.C. Wright, S.R. Shah, S.E. Amrose, A.G. Winter, A robust model of brackish water electrodialysis desalination with experimental comparison at different size scales, Desalination 443 (2018) 27-43. https://doi.org/10.1016/j.desal.2018.04.018.

[25] A.H. Galama, D.A. Vermaas, J. Veerman, M. Saakes, H.H.M. Rijnaarts, J.W. Post, K. Nijmeijer, Membrane resistance: The effect of salinity gradients over a cation exchange membrane, Journal of Membrane Science 467 (2014) 279-291. https://doi.org/10.1016/j.memsci.2014.05.046.

[26] A.M. Weiner, R.K. McGovern, J.H. Lienhard V, Increasing the power density and reducing the levelized cost of electricity of a reverse electrodialysis stack through blending, Desalination 369 (2015) 140-148. https://doi.org/10.1016/j.desal.2015.04.031.

[27] S. Pawlowski, V. Geraldes, J.G. Crespo, S. Velizarov, Computational fluid dynamics (CFD) assisted analysis of profiled membranes performance in reverse electrodialysis, Journal of Membrane Science 502 (2016) 179-190. https://doi.org/10.1016/j.memsci.2015.11.031.

[28] P. Długołęcki, P. Ogonowski, S.J. Metz, M. Saakes, K. Nijmeijer, M. Wessling, On the resistances of membrane, diffusion boundary layer and double layer in ion exchange membrane transport, Journal of Membrane Science 349 (2010)

369-379. https://doi.org/10.1016/j.memsci.2009.11.069.

[29] G.M. Geise, A.J. Curtis, M.C. Hatzell, M.A. Hickner, B.E. Logan, Salt Concentration Differences Alter Membrane Resistance in Reverse Electrodialysis Stacks, Environmental Science & Technology Letters 1 (2013) 36-39. https://doi.org/10.1021/ez4000719.

[30] H. Strathmann, Ion-exchange membrane separation processes, Elsevier (2004).

[31] A.J.B. Kemperman, Handbook bipolar membrane technology, Enschede: Twente University Press (2000).

[32] J. Pretz, E. Staude, Reverse electrodialysis (RED) with bipolar membranes, an energy storage system, Ber Bunsen Phys Chem 102 (1998) 676-685. https://doi.org/10.1002/bbpc.19981020412.

[33] L. Gurreri, A. Tamburini, A. Cipollina, G. Micale, Electrodialysis applications in wastewater treatment for environmental protection and resources recovery: a systematic review on progress and perspectives, Membranes 10 (2020). https://doi.org/10.3390/membranes10070146.

[34] J.A. Manzanares, G. Vergara, S. Mafé, K. Kontturi, P. Viinikka, Potentiometric determination of transport numbers of ternary electrolyte systems in charged membranes, The Journal of Physical Chemistry B 102 (1998) 1301-1307. https://doi.org/10.1021/jp970216w.

[35] M.L. Cerva, M.D. Liberto, L. Gurreri, A. Tamburini, A. Cipollina, G. Micale, M. Ciofalo, Coupling CFD with a one-dimensional model to predict the performance of reverse electrodialysis stacks, Journal of Membrane Science 541 (2017) 595-610. https://doi.org/10.1016/j.memsci.2017.07.030.

[36] Y. Tanaka, M. Reig, S. Casas, C. Aladjem, J.L. Cortina, Computer simulation of ion-exchange membrane electrodialysis for salt concentration and reduction of RO discharged brine for salt production and marine environment conservation, Desalination 367 (2015) 76-89. https://doi.org/10.1016/j.desal.2015.03.022.

[37] M.Z. Yang, H. Wu, J.R. Selman, A model for bipolar current leakage in cell stacks with separate electrolyte loops, Journal of applied electrochemistry 19 (1989) 247-254. https://doi.org/10.1007/BF01062308.

[38] A. Culcasi, L. Gurreri, A. Zaffora, A. Cosenza, A. Tamburini, A. Cipollina, G. Micale, Ionic shortcut currents via manifolds in reverse electrodialysis stacks, Desalination 485 (2020) 114450. https://doi.org/10.1016/j.desal.2020.114450.

[39] I. Rubinstein, J. Pretz, E. Staude, Open circuit voltage in a reverse electrodialysis cell, Physical Chemistry Chemical Physics 3 (2001) 1666-1667. https://doi.org/10.1039/B010030G.

[40] Y. Tanaka, Ion exchange membranes: fundamentals and applications, Second Edition, Membrane Science and Technology: Elsevier, Netherlands (2015).

[41] I. Rousar, V. Cezner, Experimental determination and calculation of parasitic currents in bipolar electrolyzers with application to chlorate electrolyzer, Journal of The Electrochemical Society 121 (1974) 648.

https://doi.org/10.1149/1.2401878.

[42] P. Tsiakis, L.G. Papageorgiou, Optimal design of an electrodialysis brackish water desalination plant, Desalination 173 (2005) 173-186. https://doi.org/10.1016/j.desal.2004.08.031.

[43] V.V. Nikonenko, A.V. Kovalenko, M.K. Urtenov, N.D. Pismenskaya, J. Han, P. Sistat, G. Pourcelly, Desalination at overlimiting currents: State-of-the-art and perspectives, Desalination 342 (2014) 85-106. https://doi.org/10.1016/j.desal.2014.01.008.

[44] L. Karimi, A. Ghassemi, An empirical/theoretical model with dimensionless numbers to predict the performance of electrodialysis systems on the basis of operating conditions, Water Research 98 (2016) 270-279. https://doi.org/10.1016/j.watres.2016.04.014.

[45] H.J. Lee, F. Sarfert, H. Strathmann, S.H. Moon, Designing of an electrodialysis desalination plant, Desalination 142 (2002) 267-286. https://doi.org/10.1016/S0011-9164(02)00208-4.

[46] C. Larchet, V.I. Zabolotsky, N. Pismenskaya, V.V. Nikonenko, A. Tskhay, K. Tastanov, G. Pourcelly, Comparison of different ED stack conceptions when applied for drinking water production from brackish waters, Desalination 222 (2008) 489-496. https://doi.org/10.1016/j.desal.2007.02.067.